

Development of the Truckee River terraces on the northeastern flank of the Sierra Nevada

Steven G. Wesnousky^{a,*}, Lewis A. Owen^b

^a Center for Neotectonic Studies and Nevada Seismological Laboratory, University of Nevada, Reno, 1664 North Virginia St., Reno, NV 89557, USA

^b Department of Marine, Earth, and Atmospheric Sciences, North Carolina State University, Raleigh, NC 27569, USA

ARTICLE INFO

Article history:

Received 26 May 2020

Received in revised form 23 August 2020

Accepted 24 August 2020

Available online 25 August 2020

Keywords:

Strath terraces

Sierra Nevada

Glaciation

Cosmogenic exposure age

ABSTRACT

The distribution and elevation of the abandoned strath terraces along the Truckee River in the Carson Range on the eastern flank of the Sierra Nevada are mapped and quantified with measurements from Lidar accompanied by field survey. Each mapped strath terrace is formed by incision into the Hunter Creek Sandstone and deposition of fluvial gravel by the Truckee River. The gravel contains granitic boulders sourced from the glaciated headwaters of the Truckee >20 km upstream from the terraces and display boulders ranging from 4 to 12 m in dimension, in comparison to the <1 m dimension of boulders observed in the bedload of the modern *Truckee River*. Be-10 terrestrial cosmogenic nuclide (TCN) surface exposure dating places limits on the age distribution of the strath terraces. The terrace sediments are suggested to be glacial outwash deposits, temporally linked with glacial cycles, and to record an average of ~0.3 mm/a tectonic uplift with respect to the Reno Basin over the last ~350 ka. Building upon earlier studies, the observations collected here increase the number of terrace levels previously mapped along the Truckee, provide initial quantitative bounds on the age of their formation, and further point to tectonic uplift as an important component in preserving this most extensive suite of strath terraces along the eastern flank of the Sierra Nevada.

© 2020 Elsevier B.V. All rights reserved.

1. Introduction

The lower Truckee River between Verdi and Reno in Nevada exhibits in number and length the most extensive suite of strath terraces preserved along the eastern flank of the Sierra Nevada. The Truckee River (herein simply the *Truckee*) flows from Lake Tahoe in the Sierra Nevada eastward to Pyramid Lake (Fig. 1A, B). The suite of terraces between Reno and Verdi in Nevada first gained attention in the studies of Birkeland (1964, 1968a, 1968b). He attributed the river terraces to four periods of glaciation at the headwaters of the *Truckee*: the youngest mid- to Late Pleistocene *Tioga* and *Tahoe* glacial stages manifest in well-preserved moraines and yet older *Donner* and *Hobart* glacial stages evidenced respectively in adjacent till sheets absent of moraine landforms and buried outcrop. Geologic maps of the area today generally embrace Birkeland's mapping and correlations (e.g., Ramelli et al., 2011 and Fig. 1B).

Motivated to further consider the causes contributing to development and preservation of the terraces, we here combine field observation with Lidar and ¹⁰Be terrestrial cosmogenic nuclide (TCN) dating methods to further consider the number and timing of strath terraces and their

deposits along the *Truckee*. The resulting observations reveal the existence of six distinct strath terraces, each most likely abandoned and preserved as the result of tectonic uplift, and apparently associated with periods of glaciation over the last several hundred thousand years, a period significantly longer than preserved by the presence of moraines elsewhere in the Sierra Nevada.

2. Correlation of terrace surfaces

Smooth, gently to moderately sloping terraces, alluvial fans, and pediment surfaces along the *Truckee* contrast to surrounding rugged topography (Fig. 1C). The terraces record alternating periods of incision and lateral planation. The geomorphic expression of the terrace surfaces and character of underlying deposits are detailed in Birkeland (1968a) and Bell and Garside (1987). The terrace deposits and pediment surfaces are developed on Neogene fluvial, fan-delta, and lacustrine deposits (Fig. 2) of the Hunter Creek Sandstone deposited between 11 Ma and 2.5 Ma (Trexler et al., 2000; Kelly and Secord, 2009). Alluvial fan and pediment surface deposits are generally poorly sorted angular and subangular gravel sourced from adjacent higher topography. Terrace deposits are rounded and subrounded cobble and boulder gravel. The boulder fraction is largely andesite and basalt with a subordinate fraction of granite composition derived only from upstream of the map area, reflecting the geology higher up along the *Truckee* Canyon (e.g., Henry

* Corresponding author.

E-mail addresses: wesnousky@unr.edu (S.G. Wesnousky), lewis.owen@ncsu.edu (L.A. Owen).

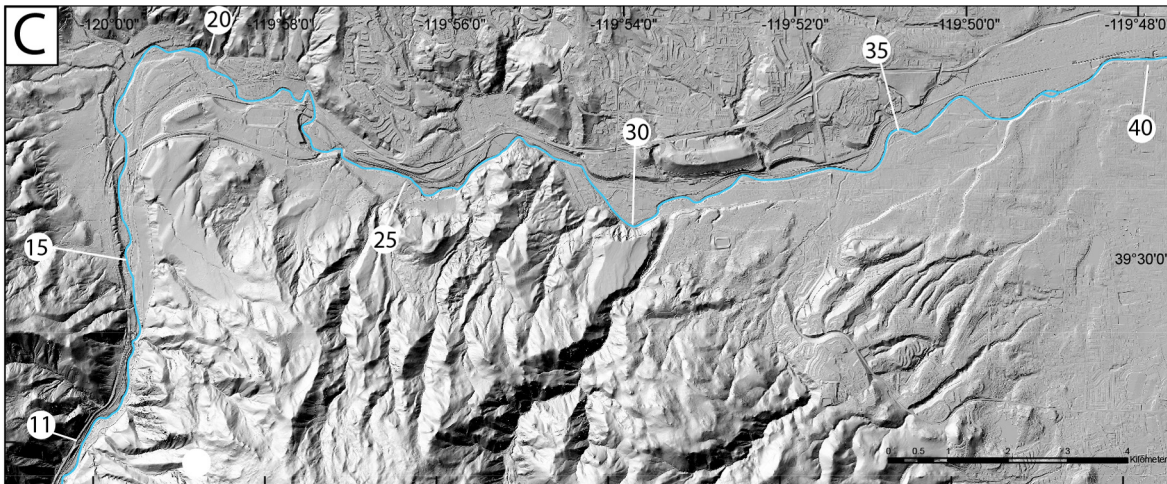
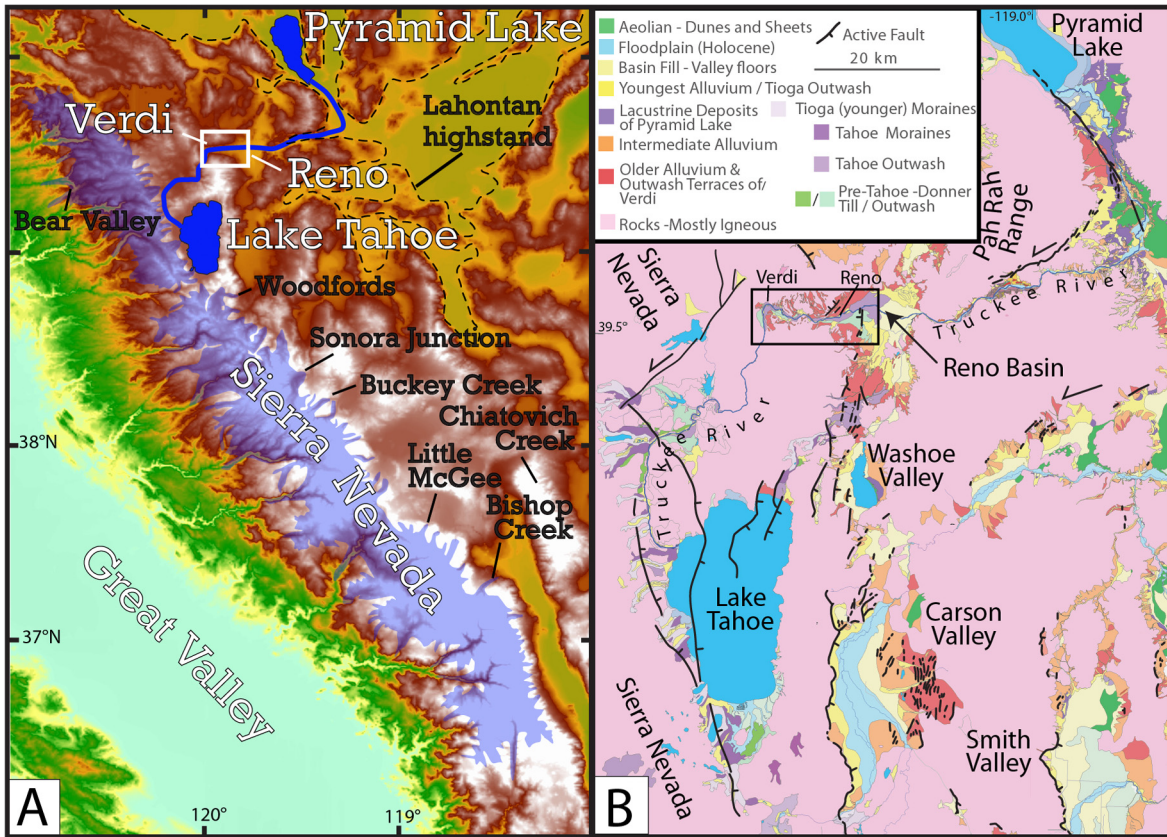




Fig. 2. Views illustrating contact separating overlying glaciofluvial gravel from underlying Hunter Creek Sandstone on mapped surfaces Q2 through Q6. Waypoints give location of contacts. Contact of gravel with Sandstone is hidden below slope debris. Thickness of gravel on Q6 is thus apparently large.

and Perkins, 2001). Reexamination of the area confirms Birkeland's (1968b) observations of the common presence of 2–3-m-diameter granite boulders on terrace surfaces, with the maximum diameter of boulders on some terraces reaching upwards of 12 m (Fig. 3). Boulders in recent alluvium along the *Truckee* are generally <1 m in diameter.

Terraces showing continuity and similar elevation above the *Truckee* stream grade are considered to share a similar age of abandonment and approximately reflect river elevation at the time of abandonment. Sloping surfaces of inactive alluvial fans and pediments likewise grade to the level of the adjacent river prior to their incision and abandonment.

Fig. 1. Location and context of study area. (A) Position of study area within the Sierra Nevada–Great Basin context (white box) on topographic base of Danielson and Gesch (2011). Extent of ice during last glacial maximum (shaded in blue and adapted from Rood et al., 2011a). The Lake Tahoe–*Truckee*–Pyramid Lake drainage shown in navy blue and pluvial Lake Lahontan highstand as a dashed line. (B) Location of terraces (black box) in context to active faults of the region (black lines) on generalized map of Quaternary deposits modified, adapted, simplified and extended from Birkeland (1963, 1964, 1968a), Sylvester et al. (2012), quadrangle maps of the region published by the Nevada Bureau of Mines and Geology (NBMG, 2020) with reference to available Lidar (USGS, 2019) and aerial photographs. (C) Hillshade image constructed from lidar-derived 1-m digital elevation model (USGS, 2019). Numbers are kilometers along the *Truckee* (blue) from arbitrary point upstream. Area of image outlined by blackbox in part B. (D) Abandoned fluvial terraces and alluvial fans pediments that graded to past levels of the *Truckee* colored as function of relative age. Stars mark sites of sampling for TCN surface exposure analysis. Numbers in stars correspond to listing of individual samples in Table 1. Waypoints and photos of each sample are archived in Supplementary Table S2 and Fig. S2.



Fig. 3. Common occurrence of fluvially transported boulders of 3–4 m in dimension with some reaching >12 m on each of the Q1 to Q6 surfaces. Q1 and Q2 images show boulders on terraces, Q4 along the terrace riser, and Q3, Q5, and Q6 images show collections of large boulders remaining in gravel pits on the respective surfaces. Waypoints of each site annotated.

Terrace surfaces judged to share the same age of abandonment are mapped and numbered Q1 (youngest) through Q6 (oldest), with notations n and s being north and south of the river, respectively (Fig. 1D). The notation p for Q6p refers to pediment surface. The correlation and measurement of terrace elevations is accomplished largely with the vertical elevation data embodied in the Lidar data (Fig. 1C). Higher terrace surfaces are interpreted to be relatively older than those lower. The degradation of terrace surface morphology with time is manifested in the smooth surfaces of the higher Q5 and Q6 surfaces observed in the field and Lidar (Fig. 1C) in contrast to well preserved bar and swale topography that remains along reaches of the lower Q1 and Q2 surfaces. Old aerial photographs (AMS, 1956) aid in the correlation of terrace surfaces where urbanization has significantly altered the landscape before the more recently collected Lidar.

Terrace elevations and heights above the active channel obtained from Lidar are plotted as a function of distance along the *Truckee* in Fig. 4. Individual measurements for consistency and reproducibility are taken primarily along abandoned terrace riser crests at points

where they are closest and strike close to parallel to the modern *Truckee* (location and values of individual measurements are recorded in supplemental Table S1).

The scatter in values for each terrace level is largely an artifact of geologic processes ranging from stream incision occurring obliquely to sloping abandoned terrace surfaces and burial by subsequent fan formation or colluviation (Supplemental Materials Fig. S1). Fig. 4 shows six sets of fluvial terraces when grouped according to elevation. The gradients of abandoned terraces generally follow the modern grade of the *Truckee*, with the exception of youngest terraces Q1 and Q2 near their eastern limit beyond kilometer ~36 where they deviate downward to merge with the current grade of the *Truckee*. Higher and older abandoned surfaces are not present downstream of kilometer 36.

The broad smooth slopes of the Q6p pediment surfaces grade to terrace Q6 and are preserved at kilometers 15, 25, and 30 along the *Truckee* (Figs. 1C and 5). The highest preserved and mapped surfaces are the Q6p fan pediments that grade to the Q6 terrace surface at kilometers 15, 25, and 30 along *Truckee* (Fig. 5). Each shares similar uniquely broad expanses

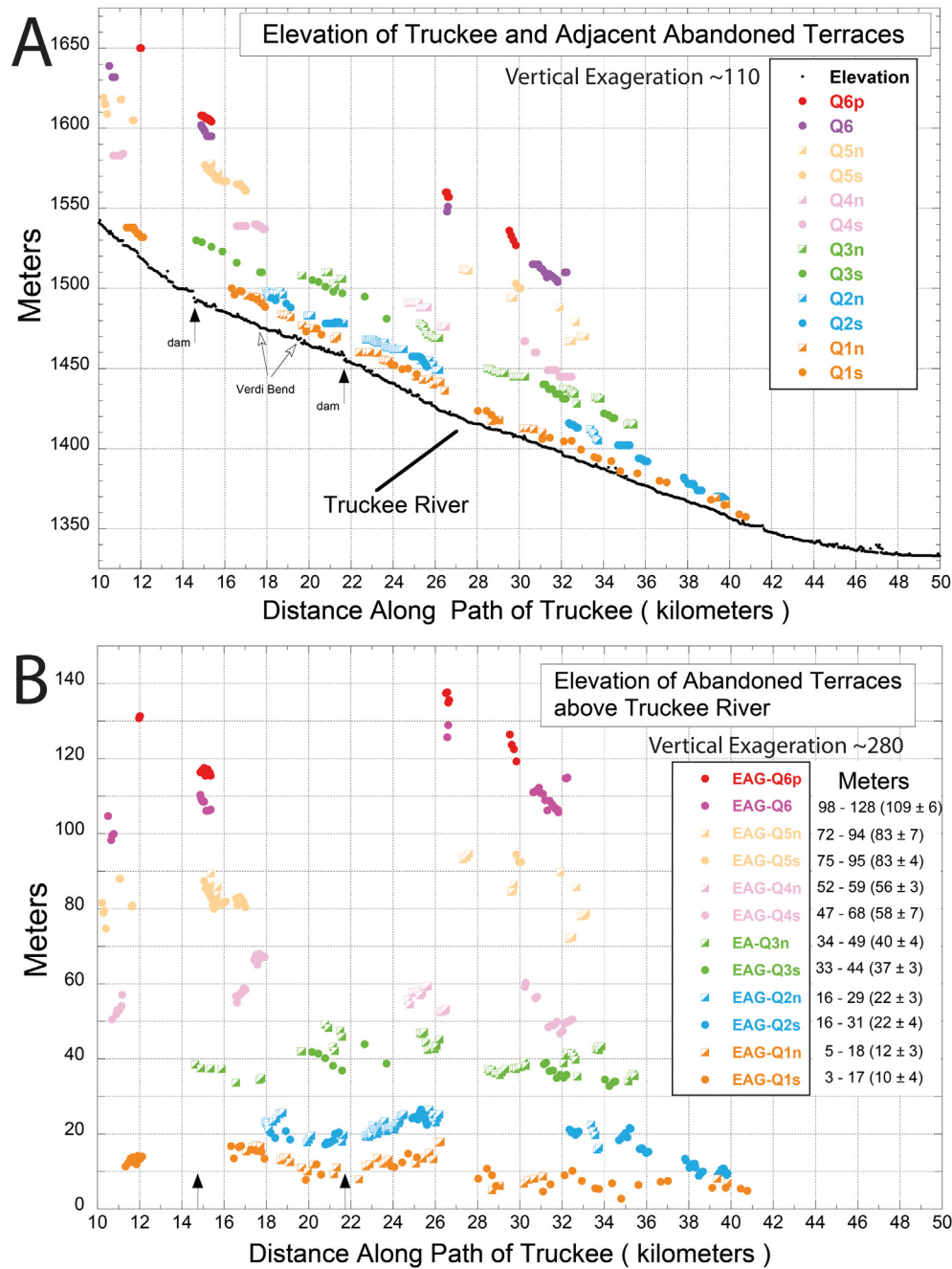


Fig. 4. Terraces along the *Truckee*. (A) Terrace elevations with distance. (B) Terrace heights above modern stream grade with range and average values tabulated at right for each terrace. Filled arrows are location of check dams on the *Truckee*. Terrace levels in (B) are locally reduced in vicinity of dams because measurements are made with respect to water level recorded in Lidar. Open arrows delineate $\sim 90^\circ$ bend in course of the *Truckee* that appears spatially associated with a change in grade of the *Truckee*. Distance along the *Truckee* measured from arbitrary point upstream. Measurements on opposite sides of the *Truckee* are labeled with n and s in the key, respectively. Measurement locations and values archived in Supplemental Materials Table S1. Geologic processes that lead to scatter in plots are described in Supplemental Materials Fig. S1.

of like geomorphic expression and similar elevation. The measured elevations of the Q6 surfaces are ~ 110 m upstream Verdi (kilometer 15) and Chalk Bluff (kilometer 30) and a higher ~ 125 m east of Belli Ranch (kilometer 25) (Fig. 5). The higher elevation measurement at Belli Ranch is somewhat of a puzzle. It may be considered that the Q6p and Q6 surfaces east of Belli Ranch records a relatively older and higher stage of the *Truckee* than preserved at Chalk Bluff and east of Belli Ranch. Alternately, the higher elevation may be an artifact of measuring the elevation of an eroded edge of a downward sloping surface. Notwithstanding this uncertainty, the terraces at the three sites are here viewed to be approximately correlative and chronicle a period of bedrock incision on the order of ~ 110 m since the *Truckee* flowed on the Q6 surface.

3. Dating of terrace surfaces

Application of TCN surface exposure dating methods to boulders and a profile of samples taken from a sediment pit provide a measure of the age of four of the six terrace surfaces. The premise and application of TCN is summarized in Gosse and Phillips (2001) and Anderson et al. (1996). Sample collection and analysis methods used here are detailed in Angster et al. (2019). In brief, samples collected are from smooth terrace surfaces exhibiting no significant erosion (gullying) and interpreted to have been stable since formation (Figs. 1C, D and S5). Each sample analyzed is derived from quartz-rich granitic rocks and estimates of ages are based on the accumulation of the ^{10}Be TCN.

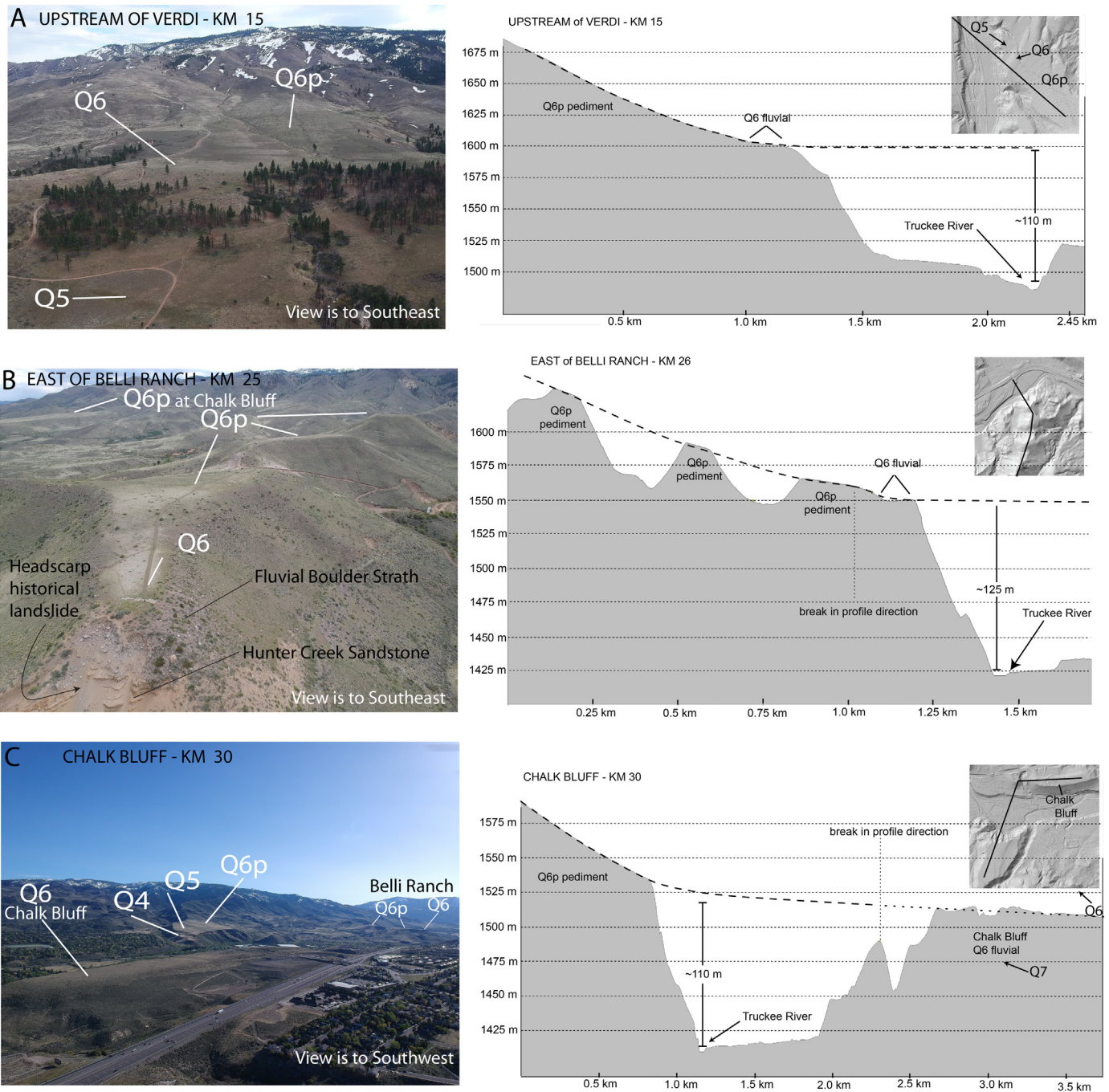


Fig. 5. Elevation measurements and observed relationship between Q6p pediment and Q6 fluvial surfaces illustrated with images (left) and profiles (right) for three locations where preserved along the *Truckee*. Black lines on small insets at right show location of profiles on hillshade images. Both images and profiles are constructed with Lidar digital elevation data. Location of sites are at kilometers 15, 25, and 30 along the course of the *Truckee* (Fig. 1C). The horizontal tonal contrasts between the Q6 and Q6p markers in 'a' are vegetation and not elevational contrasts.

Boulder samples taken from the terrace surfaces are generally the largest and apparently least weathered on the respective surfaces. Nonetheless, boulders collected on the oldest mapped surfaces typically exhibit oxidation and mineral weathering that may have removed outer boulder layers since the time of deposition. The reduction in the amount of ^{10}Be that accompanies the weathering leads to estimation of exposure ages that are minimum estimates of the age of the surface on which the boulders rest (Gosse and Phillips, 2001).

Correcting ^{10}Be TCN ages for weathering that occurs on boulder surfaces is inexact. Small et al. (1997) reports summit surfaces in the Sierra Nevada of $\sim 3 \pm 2$ m/Ma, and if we take a range of 1 to 5 m/Ma, this would result in calculated ages of 10 ka being an underestimate of

the true age by ~ 1 to 5%, an age of 50 ka by ~ 4 to 24%, and an age of 100 ka by ~ 10 to 50%. No independent measures of weathering rates exist in our study area and it is not certain that erosion rates on the summit are equivalent to rates in the study area. We present boulder ages presuming no erosion. The uncertain amount of correction that should be applied does limit though not obviate the general interpretations to be put forth here. Locations of sample sites are shown in Fig. 1D and further documented with waypoint information and photographs in supplement Table S2 and Fig. S2.

The resulting average ^{10}Be exposure ages range from ~ 29 to ~ 347 ka (Fig. 6A). Waypoints of individual boulder sample locations, chemistry of samples, and exposure age determinations are summarized in

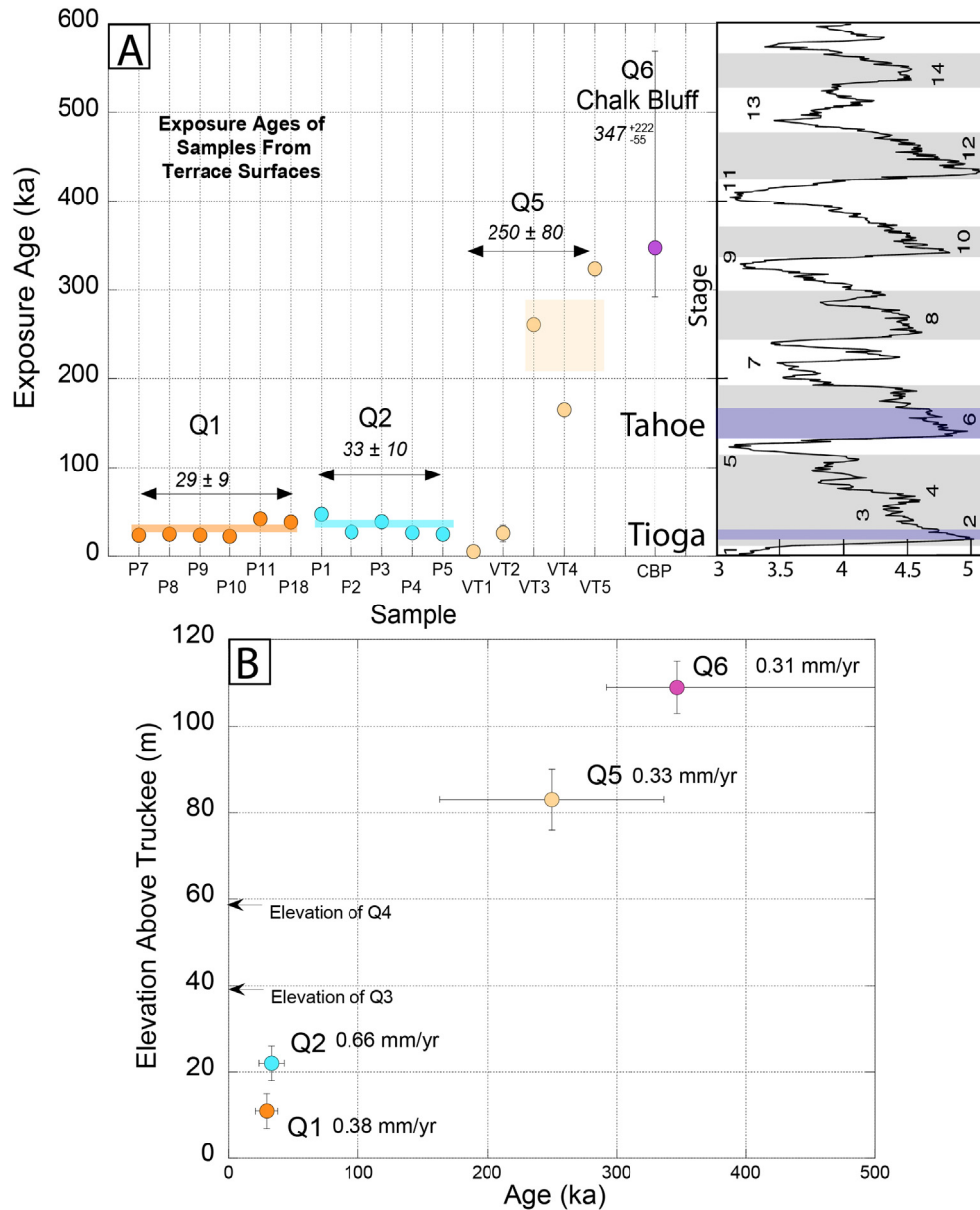


Fig. 6. Be-10 TCN surface exposure ages. (A) Ages plotted and grouped by colour according to surface sampled (e.g., Q1, Q2 ... Q6). Uncertainty bars on ages are 1σ external uncertainties output by the CRONUS-Earth online calculator for boulder samples on the Q1, Q2, and Q5 surfaces, smaller than diameter of plot symbol where not present. Uncertainty bars for the Q6 data point reflect the 2σ bounds on the age is determined with application of the Monte Carlo profile simulator of Hidy et al. (2010) that serves to provide a Bayesian best fit profile to the observed profile of ^{10}Be with depth at Chalk Bluff. Average age and 1σ (ka) of samples from respective surfaces are annotated and spanned by the transparent colored rectangles. The stacked benthic $\delta^{18}\text{O}$ records of Lisiecki and Raymo (2005) highlight the last six glacial-interglacial cycles (glacial periods are shown by grey bands). Tahoe and Tioga glacial stages mentioned in text are labeled and highlighted in dark blue. (B) Average elevation difference (between terrace surfaces and the active stream channel) as function of average age assessed for each terrace surface. Value of incision obtained by dividing average elevation differences by average age for each dated surface is annotated. The youngest two samples on Q5 surface are not included in estimates of average age.

Table 1. We here use the Lifton et al. (2014) scaling models to define ^{10}Be ages for the terraces and also provide ages using other scaling models in Table 1. Ages assessed with other scale models may vary up to ~9% (Table 1). In the absence of any surface boulders, the Q6 Chalk Bluff sample age is determined from a depth profile of ^{10}Be samples (Fig. 7). In this case, the age is determined with application of the Hidy et al. (2010) calculator, a Monte Carlo simulator that serves to provide a Bayesian best fit profile to the observed profile of ^{10}Be with depth, and the uncertainty bars for the data point in Fig. 6A reflect the 2σ bounds on the calculator's best exposure age estimate. Chemistry measurements for the Chalk Bluff profile and attendant input and output values of the Hidy et al. (2010) calculator are detailed in Supplement Table S3.

The averages of ages on each surface are annotated in Fig. 6A. Samples VT1 and VT2 are not included in the averages. These samples have

unreasonably young ages ($>3\sigma$ beyond the mean of the population), which might be attributed to erosional processes such as fire spalling or perhaps uprooting and soil disturbance that accompanies the falling of trees (Bierman and Gillespie, 1991; Dorn, 2003; Kendrick et al., 2016). Given the likelihood of surface erosion or fire spalling, it may reasonably be suggested that the oldest surface samples are more closely representative of the actual ages of the dated terrace surfaces. Albeit coupled with significant scatter in the individual ages and overlap between surfaces, the average exposure ages or the maximum sample age determined on the respective surfaces increase in a manner consistent with the relative geomorphic positions of the sampled Q1, Q2, Q5, and Q6 terrace surfaces. Descriptions and textural analyses of soil profiles may serve as a complimentary internal consistency check on TCN ages and are provided in Supplemental Materials Fig. S5 for sites on the older Q5 and Q6 surfaces.

Table 1
Sample locations, size, chemistry and ages (calculated using CRONUS v3: http://hessess.washington.edu/math/v3/v3_age_in.html).

Sample number	Quartz mass (g)	Be carrier mass (g)	Be-9 carrier concentration	North latitude (DD)	West longitude (DD)	Altitude (masl)	Sample thickness (cm)	$^{10}\text{Be}/^{9}\text{Be}$ corrected for blank (10^{-15})	Number of Be-10 (atoms/g $\text{SiO}_2 \times 10^3$)	St - Lal (1991)/Stone (2000) exposure age		Lm - Lal (1991)/Nishizumi et al. (1989) exposure age		LSDn - Lifton et al. (2014) exposure age		
										Internal uncertainty (ka)	External uncertainty (ka)	Internal uncertainty (ka)	External uncertainty (ka)	Internal uncertainty (ka)	External uncertainty (ka)	
Q1 Terrace																
P7	17.548	0.3516	1090	39.5075	119.9336	1446	2	194.1 ±	6.2 ± 283.3 ±	9.0 ± 24.0 ± 0.8	2.1	23.0 ± 0.7	1.9	23.8 ± 0.8	1.6	
P8	17.5698	0.3538	1090	39.5074	119.9338	1440	3	201.3 ±	4.9 ± 295.2 ±	7.2 ± 25.3 ± 0.6	2.1	24.2 ± 0.6	1.9	25.0 ± 0.6	1.6	
P9	16.5798	0.3542	1090	39.5075	119.9342	1439	2.5	180.0 ±	3.4 ± 280.0 ±	5.3 ± 23.9 ± 0.5	2.0	22.9 ± 0.4	1.8	23.8 ± 0.5	1.5	
P10	17.8405	0.353	1090	39.5073	119.9343	1439	3.5	182.6 ±	3.5 ± 263.1 ±	5.0 ± 22.7 ± 0.4	1.9	21.8 ± 0.4	1.7	22.6 ± 0.4	1.4	
P11	15.383	0.3549	1090	39.5075	119.9345	1435	3.5	297.9 ±	5.6 ± 500.5 ±	9.4 ± 43.4 ± 0.8	3.6	40.8 ± 0.8	3.2	42.0 ± 0.8	2.6	
P18	9.4375	0.3494	1023	39.5209	119.9804	1493	2.5	188.3 ±	6.6 ± 476.6 ±	16.7 ± 39.3 ± 1.4	3.4	37.2 ± 1.3	3.1	38.4 ± 1.4	2.7	
														Average (1 sigma uncertainty)	29.3 ± 8.6	
Q2 Terrace																
P1	16.7535	0.3523	1090	39.5087	119.9352	1444	2	372.5 ±	7.5 ± 570.4 ±	11.5 ± 48.6 ± 1.0	4.0	45.5 ± 0.9	3.6	47.2 ± 1.0	3.0	
P2	18.4562	0.3551	1090	39.5088	119.9349	1446	2	232.5 ±	5.7 ± 325.8 ±	8.0 ± 27.6 ± 0.7	2.3	26.2 ± 0.6	2.1	27.1 ± 0.7	1.7	
P3	18.294	0.3533	1090	39.5089	119.9346	1448	2.5	331.3 ±	6.3 ± 465.9 ±	8.8 ± 39.7 ± 0.8	3.3	37.6 ± 0.7	2.9	38.9 ± 0.7	2.4	
P4	16.6944	0.3502	1090	39.5089	119.9347	1451	2	209.8 ±	5.4 ± 320.5 ±	8.2 ± 27.0 ± 0.7	2.3	25.7 ± 0.7	2.1	26.6 ± 0.7	1.7	
P5	29.0974	0.3498	1023	39.5093	119.9348	1450	2	361.9 ±	11.5 ± 297.4 ±	9.4 ± 25.1 ± 0.8	2.2	24.0 ± 0.8	2.0	24.8 ± 0.8	1.7	
														Average (1 sigma uncertainty)	32.9 ± 9.7	
Q5 Terrace																
VT-1	24.7017	0.3495	1026	39.5080	119.9895	1564	3	67.7 ±	67.9 ± 65.6 ±	65.8 ± 65.8 ± 5.1 ± 5.1	5.2	5.3 ± 5.3	5.3	5.6 ± 5.6	5.6	
VT-2	27.1302	0.35	1026	39.5074	119.9886	1566	4	377.7 ±	133.7 ± 334.0 ±	118.2 ± 26.4 ± 9.4	9.6	25.1 ± 8.9	9.1	25.8 ± 9.2	9.3	
VT-3	15.1408	0.3495	1026	39.5073	119.9886	1563	2	2152.9 ±	29.3 ± 3405.5 ±	46.4 ± 282.3 ± 4.1	24.3	256.8 ± 3.7	20.9	261.1 ± 3.8	16.9	
VT-4	30.1961	0.3517	1026	39.5071	119.9893	1562	2	2716.2 ±	37.1 ± 2168.0 ±	29.6 ± 175.2 ± 2.5	14.7	161.4 ± 2.3	12.8	165.0 ± 2.4	10.4	
VT-5	16.2273	0.3506	1026	39.5060	119.9898	1559	4	2780.0 ±	41.5 ± 4116.1 ±	61.4 ± 354.1 ± 5.8	31.1	319.4 ± 5.2	26.5	323.8 ± 5.2	21.4	
														Average (1 sigma uncertainty)	250.0 ± 80.0	

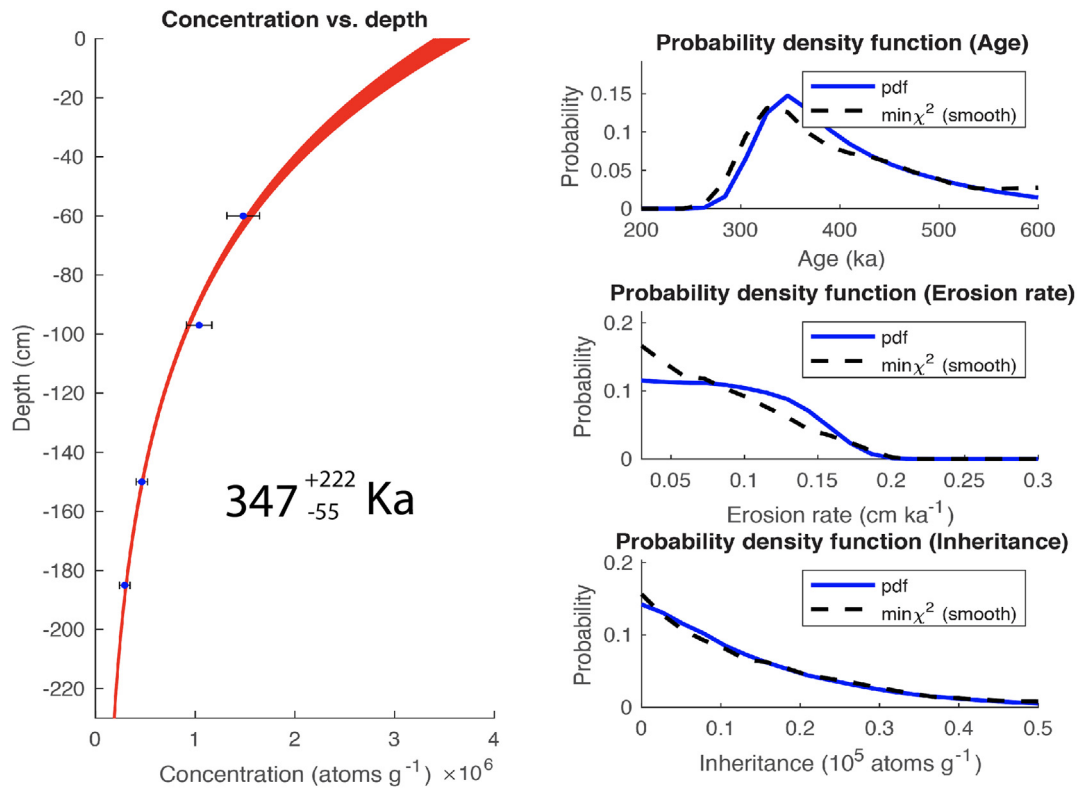


Fig. 7. Graphical output of the Hidy et al. (2010) depth profile simulator for Chalk Bluff profile. Left: Plot of the measured ^{10}Be concentration as a function of depth. The red band bounds 2σ profile solution space. Right: Probability density functions for estimates of the age, erosion rate, and inheritance that yield 2σ profile solution space. Ranges of erosion rate and inheritance provided to the calculator are not well known, which adds an unquantified degree of uncertainty to the results. Details of chemistry and input and output to simulator are in Supplementary Materials Table S3.

4. Geomorphic evolution

Viewed toward the south, the sequence of sketches in Fig. 8 illustrates the history of incision and terrace formation since the Q6p pediment surface graded to the Q6 fluvial terrace. The floodplain of the *Truckee* during Q6 time appears to have been substantially broader than today. Taking the average exposure ages to be representative of the approximate time of terrace abandonment, a period of incision dropping the *Truckee* ~25 m interrupted the period of Q6p pediment development at ~350 ka leading to abandonment of the Q6 surface. Stability of the *Truckee* again ensued until a subsequent period of incision at ~250 ka lowered the *Truckee* an additional ~25 m to abandon the Q5 surface. This same process in conjunction with hillside erosion repeated an additional four times in producing the Q4 through Q1 surfaces and today's distribution of abandoned terrace remnants. The evolution is thus one of alternating periods of incision and lateral planation and an apparent narrowing of the *Truckee* floodplain over the last ~350 ka.

5. Cause of incision

Each of the abandoned surfaces exhibit strath deposits resting on Hunter Creek Sandstone bedrock. Bedrock incision is generally considered to occur in response to a lowering of the relative base level to which rivers on now elevated terrain flow, with rates of incision modulated by changes in sediment supply and transport capacity. Climatic processes, processes of stream capture or diversion, and tectonics may result in changes in base level. The base level to which the *Truckee* flows today is Pyramid Lake (elevation of ~1160 m above sea level), a remnant of pluvial Lake Lahontan (Fig. 1A, B) that filled to ~1330 m about 15 ka (e.g., Adams and Wesnousky, 1999). The record of progressive incision recorded by the *Truckee* terraces spans a much longer period (~350 ka or more), and the ages of individual dated surfaces are all >15 ka, thus making it difficult

to attribute terrace formation to the desiccation of a climatically induced higher Pyramid Lake at ~15 ka. It is also problematic to interpret that the grade of the *Truckee* recorded by the Q6 terrace remnants that are now ~110 m higher extended continuously eastward across the Reno basin. At this elevation there is no other clear path to Pyramid Lake that maintains a downward grade (Supplemental Materials Fig. S3), nor are reports of riverine or valley-fill deposits perched upwards of 100 m along the perimeter of the Reno basin.

Observations point more likely to tectonic uplift of the Sierras with respect to subsidence of the Reno Basin (Fig. 1B) as the cause of base-level change driving long-term incision along the course of the mapped terraces. Well defined east-dipping active Sierra Nevada range-bounding normal faults are present immediately to the north and south of Reno (Fig. 1A, B). The pattern of active faults where the *Truckee* enters the Reno basin differs, consisting of distributed grabens rather than a single east-facing normal scarp (Fig. 1D). The distinctive pattern of active faults was early pointed out by Thompson and White (1964) and deformation across the range front here appears to be primarily the result of distributed faulting and warping rather than a single range-bounding fault. The faults correlate spatially with the presence of a sedimentary basin that reaches to >1 km depth (Supplemental Materials Fig. S4) inferred from gravity measurements (Abbott and Louie, 2000). The localized though distributed nature of faults and warping serves to explain why the eastward extent of preservation is not the same for all terrace remnants and the apparent downward warping of the youngest Q2 and Q1 surfaces downstream of kilometer ~36 (Fig. 4A). Interpreting that terrace elevations are a result of tectonic uplift, the average rate of incision and relative uplift of the oldest 350^{+222}_{-55} ka age surface that now sits ~110 m above the *Truckee* has been $\sim 0.3^{+0.7}_{-0.1}$ mm/a. The value falls within the range of modal values of uplift rates assessed from the offset of late Pleistocene moraines by range front faults nearby at Woodfords, Buckeye Creek and Sonora Junction reported by Rood et al. (2011b) (Fig. 1A). The similarity

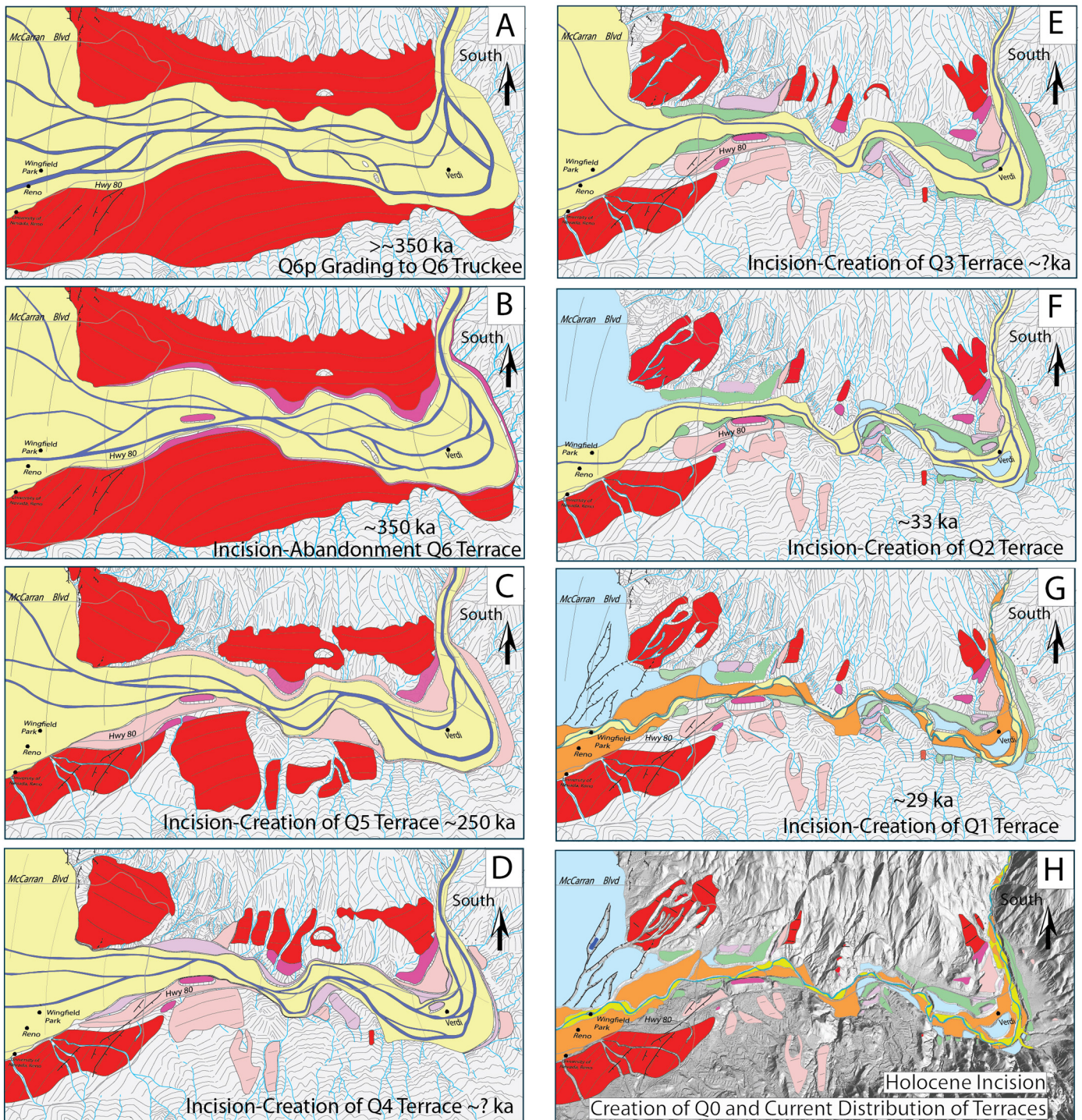


Fig. 8. Sequential evolution of Truckee River terraces viewed obliquely from the south. Panels are arranged from oldest (A) to youngest (H). Map unit colors follow those in Fig. 1D. Depiction commences with interpretation that Q6p was largely continuous and graded to the Truckee prior to ~350 ka. Incision and lateral planation and erosion of existing abandoned terrace remnants occurs during time between panels.

of gradients of terrace remnants suggests a rather block-like uplift, but for the warping associated with distributed faulting between kilometers ~36 to 40. (Fig. 4A). Confidence in any assertion that the uplift rates at Reno have been steady or changed over time of terrace development is compromised by the uncertainties in age estimates.

6. Potential record of glaciation

Each of the strath terrace deposits has boulders in dimension ranging commonly from >2–3 m and up to 12 m dimension, beyond

the smaller <1-m-diameter boulders present along the same reaches of the present-day Truckee. Birkeland (1968b) interpreted that the terraces record discharges and flow velocities to have been much greater than today and that the largest boulders were commonly granite with potential source areas upstream of the map area, likely the headwaters of the Truckee. He further suggested that the large boulder deposits were the result of glacial lake outburst floods (GLOFs) caused by failure of glacial ice dams that crossed the upper Truckee canyon and temporarily raised the level of Lake Tahoe. Similarly, Blair (2001) and Benn et al. (2006) argue for the importance of GLOFs as formative processes in producing

alluvial fans along the eastern Sierra Nevada in Owens Valley. Whether or not it is this process that is responsible for all of the strath deposits, the large size of clasts and the presence of boulders of Sierran granite make for the reasonable suggestion that each of the strath deposits corresponds to periods of increased flow and transport that accompany periods of glaciation. In this context, the alternation of periods of lateral beveling versus vertical incision required to produce the *Truckee* terrace sequence appear linked to changes in sediment flux over glacial cycles. Similar linkages of landform development to major stages of glaciation have also been observed around the globe in the western United States (Bull, 1977; Wells et al., 1987; Wells et al., 1990; Bull, 1991; Harvey et al., 1999; Bull, 2000; Blair, 2001), the Tibetan Plateau (Owen et al., 2006; Blothe et al., 2014; Gao et al., 2016; Wang et al., 2017; Hu et al., 2018), High Atlas Mountains in Morocco (Arbolea et al., 2008; Pastor et al., 2015), the Indian Himalaya (Ray and Srivastava, 2010; Dosseto et al., 2018; Shukla et al., 2018), Khumbu Himal (Barnard et al., 2006), Kyrgyz Then Shan (Burgette et al., 2017), and the Danube valley of Austria (Ruszkiczay-Rudiger et al., 2016), and thus give further reason to the idea that terrace development along the *Truckee* is related to glacial cycles.

The chronology of Late Pleistocene glaciation in the Sierra Nevada is formulated primarily on TCN surface exposure dating of moraines (Phillips et al., 1990; Phillips et al., 1996; James, 2002; Phillips et al., 2009; Rood et al., 2011a; Wesnousky et al., 2016; Pierce et al., 2017). The extensive survey of Rood et al. (2011a) along the east flank of the Sierra Nevada south of about Lake Tahoe places retreat of the maximum glacial advances at ~19 and ~140 ka for the last two glacial cycles. Moraines along a few singular drainages have been interpreted to suggest that major advances also occurred between these periods. Phillips et al. (1996, 2009) date moraines at Chiatovich and Bishop creeks at ~25–27 ka and two sets of moraines at Little McGee Creek (Fig. 1A) to ~32 and ~50 ka (Fig. 1A). James (2002) interpret two sets of moraines in Bear Valley to have formed at ~49 and ~76 ka. The possibility exists that the history of glacial advances is not shared along the length of the Sierra Nevada. Alternatively, end-moraine positions of major marine oxygen isotope stages (MIS) 2 and 6 glaciations are about the same and the disparate record of moraines between these times has reasonably been attributed to their obliteration during major advances of MIS 2 (Gillespie and Zhefuss, 2004). In this context of prior studies, the uncertainty and older ages determined for the Q5 and Q6 surfaces preclude unique comparison to earlier glacial times, while the younger ages of the Q1 and Q2 surfaces might be associated with ages of moraines recognized elsewhere in the Sierra Nevada. That said, the current inability to uniquely distinguish between the ages of the Q1 and Q2 surfaces leaves open the possibility that they do not correspond to separate major stages of glaciation and processes other than major glacial cycles have also played a role in formation of the terraces.

7. Interplay between tectonics, glaciation, and terrace preservation

The number and extent of terraces near Reno is significantly greater than observed in other drainages that debouch from the eastern flank of the Sierra Nevada. The observation is ascribed to unique geographic circumstance. Moraines along the east flank of the Sierra Nevada generally extend in narrow canyons to a steep normal-faulted range front, such that younger glacial advances may remove older ones on the footwall and normal fault displacement aids burial of distal moraine and outwash deposits on the hanging wall. In contrast, the limit of ice and moraine formation at the headwaters of the *Truckee* is separated from the locus of range front uplift at Reno by the Truckee Canyon. Glacial outwash debouches near Verdi and is deposited over a long stretch of the range front footwall. Range front uplift thus serves to preserve and separate outwash deposits from different periods of time. The resolution of the terrace record formed in this manner must be limited to some degree by the rate of uplift. Uplift will be insufficient to result in preservation of separate terraces if periods of increased outwash are spaced too closely

in time. Conversely, the distinct separation of terraces along the Verdi-Reno corridor indicates significant and discrete periods of time between outwash events.

8. Conclusion

The observations assembled here increase the number of terrace levels previously recognized along the *Truckee*, provide initial quantitative bounds on the age of their formation, and introduce tectonic uplift as an important component in creating and preserving the most extensive suite of fluvial terraces along the eastern flank of the Sierra Nevada. Specifically, the presence of six terraces and their deposits along a 40-km-reach of the *Truckee* records an ~350 ka period of incision and relative uplift caused by faulting along the Sierra Nevada range front equal to ~0.3 mm/a. Interpretation that the terrace deposits are glacial outwash all or in part caused by glacial outburst floods suggests a direct linkage of terrace formation to glacial cycles, albeit chronologic data alone remain at present insufficient to definitively prove the correlation.

Declaration of competing interest

The authors declare that they have no known competing financial interests or personal relationships that could have appeared to influence the work reported in this paper.

Acknowledgments

In the steps of Peter Birkeland. Assistance in collection and sample preparation was in part provided by P. Jayangaperumal and I. Pierce. Ken Adams, Doug Burbank, Craig Jones, and Marith Reheis provided constructive comments on an initial version of the manuscript. The presentation has subsequently benefited from the comments of three anonymous reviewers. Center for Neotectonics Studies Contribution No. 80.

Appendix A. Supplementary data

Supplementary data to this article can be found online at <https://doi.org/10.1016/j.geomorph.2020.107399>.

References

- Abbott, R.E., Louie, J.N., 2000. Depth to bedrock using gravimetry in the Reno and Carson City, Nevada, area basins. *Geophysics* 65 (2), 340–350.
- Adams, K.D., Wesnousky, S.G., 1999. The Lake Lahontan highstand: age, surficial characteristics, soil development, and regional shoreline correlation. *Geomorphology* 30 (4), 357–392.
- AMS, 1956. Photos 230 - 234 of American Mapping Service (AMS) flight lines HY M 2 21 Nov. 56 160 Are Used in This Study to Compliment More Recent Lidar in Areas Where Urbanization Has Obscured Original Geomorphology.
- Anderson, R.S., Repka, J.L., Dick, G.S., 1996. Explicit treatment of inheritance in dating depositional surfaces using in situ Be-10 and Al-26. *Geology* 24 (1), 47–51.
- Angster, S.A., Wesnousky, S.G., Figueiredo, P., Owen, L.A., Hammer, S., 2019. Late Quaternary slip rates for faults of the Central Walker Lane: Spatiotemporal strain release in a strike-slip fault system. *Geosphere* 15 (5), 1460–1478. <https://doi.org/10.1130/GES02088.1>.
- Arbolea, M.L., Babault, J., Owen, L.A., Teixell, A., Finkel, R.C., 2008. Timing and nature of Quaternary fluvial incision in the Ouarzazate foreland basin, Morocco. *J. Geol. Soc.* 165, 1059–1073.
- Barnard, P.L., Owen, L.A., Finkel, R.C., 2006. Quaternary fans and terraces in the Khumbu Himal south of Mount Everest: their characteristics, age and formation. *J. Geol. Soc.* 163, 383–399.
- Bell, J.W., Garside, L.J., 1987. Verdi Quadrangle: Geologic Map Urban Map 4Gg. Nevada Bureau of Mines and Geology, Nevada.
- Benn, D.I., Owen, L.A., Finkel, R.C., Clemmens, S., 2006. Pleistocene lake outburst floods and fan formation along the eastern Sierra Nevada, California: implications for the interpretation of intermontane lacustrine records. *Quat. Sci. Rev.* 25 (21–22), 2729–2748.
- Bierman, P., Gillespie, A., 1991. Range fires - a significant factor in exposure-age determination and geomorphic surface evolution. *Geology* 19 (6), 641–644.
- Birkeland, P.W., 1963. Pleistocene volcanism and deformation of the Truckee area, north of Lake Tahoe, California. *Geological Society of America Bulletin* 74, 1453–1464.
- Birkeland, P.W., 1964. Pleistocene glaciation of the northern Sierra Nevada, north of Lake Tahoe, California. *J. Geol.* 72 (6), 810–825.

- Birkeland, P.W., 1968a. Correlation of Quaternary stratigraphy of the Sierra Nevada with that of the Lake Lahontan area. In: Morrison, R.B., Wright, H.E.J. (Eds.), *INQUA Congress, 7th*, University of Utah Press, Salt Lake City, Boulder, Colorado, pp. 469–499
- Birkeland, P.W., 1968b. Mean velocities and boulder transport during Tahoe-age floods of Truckee River California-Nevada. *Geological Society of America Bulletin* 79 (1), 137–141.
- Blair, T.C., 2001. Outburst flood sedimentation on the proglacial Tuttle Canyon alluvial fan, Owens Valley, California, USA. *J. Sediment. Res.* 71 (5), 657–679.
- Blothe, J.H., Munack, H., Korup, O., Fulling, A., Garzanti, E., Resentini, A., Kubik, P.W., 2014. Late Quaternary valley infill and dissection in the Indus River, western Tibetan Plateau margin. *Quat. Sci. Rev.* 94, 102–119.
- Bull, W.B., 1977. The alluvial-fan environment. *Progress in Physical Geography* 1, 222–270.
- Bull, W.B., 1991. *Geomorphic Responses to Climatic Change*. Oxford University Press, New York.
- Bull, W.B., 2000. Correlation of fluvial aggradation events to times of global climate change. In: Noller, J.S., Sowers, J.M., Lettis, W.R. (Eds.), *Quaternary Geochronology: Methods and Applications*. American Geophysical Union, Washington, D.C, pp. 456–464.
- Burgette, R.J., Weldon, R.J., Abdrakhatov, K.Y., Ormukov, C., Owen, L.A., Thompson, S.C., 2017. Timing and process of river and lake terrace formation in the Kyrgyz Tien Shan. *Quat. Sci. Rev.* 159, 15–34.
- Danielson, J.J., Gesch, D.B., 2011. Global multi-resolution terrain elevation data 2010 (GMTED2010). Earth Resources Observation and Science (EROS) Center, Earth Resources Observation and Science Center, OFR 2011-1073. https://www.usgs.gov/centers/eros/science/usgs-eros-archive-digital-elevation-global-multi-resolution-terrain-elevation?qt-science_center_objects=3#qt-science_center_objects.
- Dorn, R.L., 2003. Boulder weathering and erosion associated with a wildfire, Sierra Ancha Mountains, Arizona. *Geomorphology* 55 (1–4), 155–171.
- Dosseto, A., May, J.H., Choi, J.H., Swander, Z.J., Fink, D., Korup, O., Hesse, P., Singh, T., Mifsud, C., Srivastava, P., 2018. Late quaternary fluvial incision and aggradation in the Lesser Himalaya, India. *Quat. Sci. Rev.* 197, 112–128.
- Gao, H.S., Li, Z.M., Ji, Y.P., Pan, B.T., Liu, X.F., 2016. Climatic and tectonic controls on strath terraces along the upper Weihe River in central China. *Quat. Res.* 86 (3), 326–334.
- Gillespie, A.R., Zhefuss, P.H., 2004. Glaciations of the Sierra Nevada, California, USA. In: Ehlers, J., Gibbard, P.L. (Eds.), *Quaternary Glaciations*, pp. 51–62.
- Gosse, J.C., Phillips, F.M., 2001. Terrestrial in situ cosmogenic nuclides: theory and application. *Quat. Sci. Rev.* 20 (14), 1475–1560.
- Harvey, A.M., Wigand, P.E., Wells, S.G., 1999. Response of alluvial fan systems to the late Pleistocene to Holocene climatic transition: contrasts between the margins of pluvial Lakes Lahontan and Mojave, Nevada and California, USA. *Catena* 36 (4), 255–281.
- Henry, C.D., Perkins, M.E., 2001. Sierra Nevada-Basin and Range transition near Reno, Nevada: two-stage development at 12 and 3 Ma. *Geology* 29 (8), 719–722.
- Hidy, A.J., Gosse, J.C., Pedersen, J.L., Mattern, J.P., Finkel, R.C., 2010. A geologically constrained Monte Carlo approach to modelling exposure ages from profiles of cosmogenic nuclides: an example from Lees Ferry, Arizona. *Geochemistry, Geophysics, Geosystems* 11 (2 Sept). <https://doi.org/10.1029/2010GC003084> 18 pp.
- Hu, H.P., Feng, J.L., Chen, F., 2018. Sedimentary records of a palaeo-lake in the middle Yarlung Tsangpo: implications for terrace genesis and outburst flooding. *Quat. Sci. Rev.* 192, 135–148.
- James, L.A., 2002. Late Pleistocene glaciations in the northwestern Sierra Nevada, California. *Quat. Res.* 57, 409–419.
- Kelly, T.S., Secord, R., 2009. Biostratigraphy of the Hunter Creek Sandstone, Verdi Basin, Washoe County, Nevada. In: Oldow, J.S., Cashman, P. (Eds.), *Late Cenozoic Structure and Evolution of the Great Basin-Sierra Nevada Transition*, pp. 133–146.
- Kendrick, K.J., Partin, C.A., Graham, R.C., 2016. Granitic boulder erosion caused by chaparral wildfire: implications for cosmogenic radionuclide dating of bedrock surfaces. *J. Geol.* 124 (4), 529–539.
- Lal, D., 1991. Cosmic-ray labeling of erosion surfaces - in situ nuclide production-rates and erosion models. *Earth Planet. Sci. Lett.* 104 (2–4), 424–439.
- Lifton, N., Sato, T., Dunai, T.J., 2014. Scaling in situ cosmogenic nuclide production rates using analytical approximations to atmospheric cosmic-ray fluxes. *Earth and Planetary Science Letters* 386, 149–160.
- Lisiecki, L.E., Raymo, M.E., 2005. A Plio-Pleistocene stack of 57 globally distributed benthic $\delta^{18}O$ records. *Paleoceanography* 20, 17. <https://doi.org/10.1029/2004PA001071>.
- NBMG, 2020. Nevada Bureau of Mines and Geology Maps and Data. <http://www.nbmgs.unr.edu/Maps&Data/>.
- Nishiizumi, K., Winterer, E.L., Kohl, C.P., Klein, J., Middleton, R., Lal, D., Arnold, J.R., 1989. Cosmic-ray production-rates of Be-10 and Al-26 in quartz from glacially polished rocks. *J. Geophys. Res. Solid Earth Planets* 94 (B12), 17907–17915.
- Owen, L.A., Finkel, R.C., Haizhou, M., Barnard, P.L., 2006. Late Quaternary landscape evolution in the Kunlun Mountains and Qaidam Basin, Northern Tibet: a framework for examining the links between glaciation, lake level changes and alluvial fan formation. *Quat. Int.* 154, 73–86.
- Pastor, A., Babault, J., Owen, L.A., Teixell, A., Arboleya, M.L., 2015. Extracting dynamic topography from river profiles and cosmogenic nuclide geochronology in the Middle Atlas and the High Plateaus of Morocco. *Tectonophysics* 663, 95–109.
- Phillips, F.M., Zreda, M.G., Smith, S.S., Elmore, D., Kubik, P.W., Sharma, P., 1990. Cosmogenic Chlorine-36 chronology for glacial deposits at Bloody Canyon, Eastern Sierra-Nevada. *Science* 248 (4962), 1529–1532.
- Phillips, F.M., Zreda, M.G., Benson, L.V., Plummer, M.A., Elmore, D., Sharma, P., 1996. Chronology for fluctuations in late Pleistocene Sierra Nevada glaciers and lakes. *Science* 274 (5288), 749–751.
- Phillips, F.M., Zreda, M., Plummer, M.A., Elmore, D., Clark, D.H., 2009. Glacial geology and chronology of Bishop Creek and vicinity, eastern Sierra Nevada, California. *Geological Society of America Bulletin* 121 (7–8), 1013–1033.
- Pierce, I.K.D., Wesnously, S.G., Owen, L.A., 2017. Terrestrial cosmogenic surface exposure dating of moraines at Lake Tahoe in the Sierra Nevada, California, and slip rate estimate for the Wet Tahoe fault. *Geomorphology* 298, 63–71.
- Ramelli, A.R., Henry, C.D., Walker, J.P., 2011. Preliminary Revised Geologic Maps of the Reno Urban Area, Nevada, Plates 1, 2, and 3: Open-file Report 11-7. Nevada Bureau of Mines and Geology.
- Ray, Y., Srivastava, P., 2010. Widespread aggradation in the mountainous catchment of the Alaknanda-Ganga River System: timescales and implications to Hinterland-foreland relationships. *Quat. Sci. Rev.* 29 (17–18), 2238–2260.
- Rood, D.H., Burbank, D.W., Finkel, R.C., 2011a. Chronology of glaciations in the Sierra Nevada, California, from Be-10 surface exposure dating. *Quat. Sci. Rev.* 30 (5–6), 646–661.
- Rood, D.H., Burbank, D.W., Finkel, R.C., 2011b. Spatiotemporal patterns of fault slip rates across the central Sierra Nevada frontal fault zone. *Earth and Planetary Science Letters* 301 (3–4), 457–468.
- Ruszkiczay-Rudiger, Z., Braucher, R., Novothny, A., Csillag, G., Fodor, L., Molnar, G., Madarasz, B., Team, A., 2016. Tectonic and climatic control on terrace formation: coupling in situ produced Be-10 depth profiles and luminescence approach, Danube River, Hungary, Central Europe. *Quat. Sci. Rev.* 131, 127–147.
- Shukla, T., Mehta, M., Jaiswal, M.K., Srivastava, P., Dobhal, D.P., Nainwal, H.C., Singh, A.K., 2018. Late Quaternary glaciation history of monsoon-dominated Dingad basin, central Himalaya, India. *Quat. Sci. Rev.* 181, 43–64.
- Small, E.E., Anderson, R.S., Repka, J.L., Finkel, R., 1997. Erosion rates of alpine bedrock summit surfaces deduced from in situ Be-10 and Al-26. *Earth Planet. Sci. Lett.* 150 (3–4), 413–425.
- Stone, J.O., 2000. Air pressure and cosmogenic isotope production. *J. Geophys. Res.-Solid Earth* 105 (B10), 23753–23759.
- Sylvester, A.G., Wise, W.W., Hasting, J.T., Moyer, A., 2012. Geologic Map of the North Lake Tahoe - Donner Pass region, Northern Sierra Nevada, California, California Geological Survey Map Sheet 60. California Geological Survey, California Department of Conservation, Sacramento, California.
- Thompson, G.A., White, D.E., 1964. Regional geology of the Steamboat Springs area, Washoe County, Nevada. U. S. Geological Survey Professional Paper, 458-A 52p.
- Trexler, J.H., Cashman, P.H., Henry, C.D., Muntean, T., Schwartz, K., Ten-Brink, A., Faulds, J.E., Perkins, M., Kelly, T., 2000. Neogene basins in western Nevada document the tectonic history of the Sierra Nevada-Basin and Range transition zone for the last 12 Ma. In: Lageson, D.R. (Ed.), *Great Basin and Sierra Nevada*. Geological Society of America, Boulder, Colorado, pp. 97–116.
- USGS, 2019. The National Map, 3DEP products and services: the National Map 3D elevations program web page. at: https://nationalmap.gov/3DEP/3dep_prodserv.html. (Accessed March 2019).
- Wang, Z.J., Meyer, M.C., Gliganic, L.A., Hoffmann, D.L., May, J.H., 2017. Timing of fluvial terrace formation and concomitant travertine deposition in the upper Sutlej River (Tirthapur, southwestern Tibet) and paleoclimatic implications. *Quat. Sci. Rev.* 169, 357–377.
- Wells, S.G., McFadden, L.D., Dohrenwend, J.C., 1987. Influence of late Quaternary climatic changes on geomorphic and pedogenic processes on a desert piedmont, eastern Mojave Desert, California. *Quat. Res.* 27 (2), 130–146.
- Wells, S.G., McFadden, L.D., Harden, J., 1990. Preliminary results of age estimations and regional correlations of Quaternary alluvial fans within the Mojave Desert of Southern California. In: Reynolds, R.E., Wells, S.G., Brady, R.J.I. (Eds.), *At the End of the Mojave: Quaternary Studies in the Eastern Mojave Desert*. Special Publications of the San Bernardino County Museum Association, Redlands, CA, pp. 45–53.
- Wesnously, S.G., Briggs, R.W., Caffee, M.C., Ryerson, F.J., Finkel, R., Owen, L.A., 2016. Terrestrial cosmogenic surface exposure dating of glacial and associated landforms in the Ruby Mountains-East Humboldt Range of central Nevada and along the north-eastern flank of the Sierra Nevada. *Geomorphology* 268, 72–81.